Chinese Journal of Health Management
Volume 20 Issue 3, Year of Publication 2026, Page 762-779 | DoI-10.5281/zenodo.20383974

ISSN: 1674-0815

Chinese Journal of Health Management

Chinese Medical Association

Formulation and Evaluation of Silver Nanoparticles from Aloe Barbadensis Leaves extract for Antimicrobial activity

Babasaheb V. Bhagat*[1], Anil R. Pawar[2], Santosh N. Belhekar[3], Kiran K. Shinde[4], Satish M. Dhonde[5], Rajkumar S. Bagali[6], Akanksha M. Kamble[7]

[1]Associate Professor, Dr.V.V.P.F's College of Pharmacy, Ahilyanagar, Maharashtra, India, 414111
[2]Professor, Mula Education Society's College of Pharmacy, Sonai, Newasa, Ahilyanagar, Maharashtra, India, 414105
[3]Professor, Gourishankar Institute of Pharmaceutical Education and Research, Limb, Satara, Maharashtra, India, 415015
[4]Associate Professor, Vidy Niketan Institute of Pharmacy and Research Centre, Bota, Sangamner, Maharashtra, India, 422602
[5]Assistant Professor, S.V.N.H. College of Pharmacy, Shrishivajinagar, Rahuri, Ahilyanagar, Maharashtra, India, 413706
[6]Professor, Annasaheb Dange College of B Pharmacy, Ashta, Sangli, Maharashtra, India, 416301
[7]Assistant Professor, Srujan Foundation's G.D. Burkule Institute of Research in Education and Pharmaceutical Sciences, Nashik, Maharashtra, India, 422008

Article Information
Received: 11-12-2025
Revised: 18-01-2026
Accepted: 13-02-2026
Published: 28-03-2026

Keywords
Aloe barbadensis, Silver nanoparticles, Nanocarrier, Entrapment efficiency, Drug release, Stability study, Antimicrobial activity.

ABSTRACT:

The present study focused on the development and optimization of Aloe barbadensis– mediated silver nanoparticles as a novel drug delivery system with improved stability, controlled release, and antimicrobial efficacy. The nanoparticles were synthesized using Aloe barbadensis extract as a natural reducing and stabilizing agent, and a 3^2 factorial design was applied to optimize formulation variables. Characterization studies confirmed particle size, zeta potential, entrapment efficiency, and surface morphology, while FTIR, XRD, and SEM analyses demonstrated successful nanoparticle formation and structural stability. The optimized formulation (F5) exhibited a particle size of 187.6 nm, zeta potential of –25.1 mV, entrapment efficiency of 84.7%, and cumulative drug release of 94.8% at 12 hours, indicating sustained release behavior. Statistical model validation showed strong agreement between predicted and experimental values, with relative error below 1%. Stability analysis revealed minimal changes under refrigerated conditions, while accelerated storage induced moderate variations. Antimicrobial testing demonstrated significant inhibition zones of 18 mm against *Escherichia coli* and 22 mm against *Staphylococcus aureus*, highlighting potent antibacterial activity. Overall, the results indicate that Aloe

barbadensis–mediated silver nanoparticles represent a promising nanocarrier platform with potential for drug delivery and infection management, warranting further in-vivo and clinical investigation.

INTRODUCTION:

Nanotechnology, a rapidly evolving interdisciplinary science, deals with the manipulation and engineering of materials at the nanometer scale, typically ranging from 1 to 100 nm, where unique physicochemical, optical, and biological properties emerge that are not observed in their bulk counterparts. In the biomedical domain, nanotechnology has opened unprecedented opportunities, including targeted drug delivery, regenerative medicine, biosensors, imaging, and antimicrobial therapies. Among various engineered nanomaterials, metallic nanoparticles, particularly silver nanoparticles, have gained significant attention due to their potent antimicrobial, anti-inflammatory, and wound-healing properties. Thus, the integration of nanotechnology into biomedical applications represents a paradigm shift in modern medicine, offering sustainable and effective strategies to address challenges such as antimicrobial resistance, poor solubility of drugs, and limited therapeutic efficacy of conventional formulations [1]. Nanotechnology refers to the manipulation, characterization, and application of materials at the nanometer scale, generally within 1–100 nm, where matter exhibits unique size-dependent physical, chemical, and biological properties. At this extremely small dimension, materials behave differently compared to their bulk form due to the dominance of quantum mechanical effects and the high surface-area-to-volume ratio. The reduction in particle size to the nanoscale drastically increases the proportion of atoms present on the surface, which enhances surface reactivity, catalytic potential, solubility, and interaction with biomolecules. Quantum confinement further influences optical, electrical, and magnetic properties, allowing for tunable fluorescence, conductivity, and energy band structures that are not achievable in macro- or microscale materials [2]. The conceptual foundation of nanotechnology was first envisioned by physicist Richard Feynman in 1959 during his lecture “There’s Plenty of Room at the Bottom,” where he described the possibility of manipulating and assembling atoms and molecules individually. The progress of the field accelerated with the development of enabling tools such as the scanning tunneling microscope (STM) and atomic force microscope (AFM) in the 1980s, which allowed visualization and manipulation at the atomic scale. Today, nanotechnology is regarded as a multidisciplinary field, integrating principles of physics, chemistry, biology, engineering, and medicine to develop novel functional materials with broad applications. Metallic nanoparticles, particularly silver, gold, and iron oxide, are among the most widely studied due to their superior physicochemical stability, tunable surface plasmon resonance, and biomedical compatibility. At the nanoscale, these metallic structures exhibit remarkable antimicrobial, anticancer, and antioxidant activities, making them potential candidates for therapeutic and diagnostic applications [3]. Nanotechnology has grown into a global research frontier supported by major initiatives such as the U.S. National Nanotechnology Initiative (NNI), the European Union’s Nanosciences program, and national nanomission projects in countries including India, Japan, and China. Investments in nanoscience and nanotechnology research continue to rise due to their transformative impact across multiple sectors, including electronics, energy storage, food science, textiles, agriculture, and medicine. Biomedical sciences, in particular, have benefitted significantly from nanoscale innovations. Nanoparticles can be engineered for targeted drug delivery, diagnostic imaging, biosensing, and regenerative medicine. Their small size enables them to penetrate cellular barriers, interact with intracellular structures, and even cross the blood–brain barrier, which is a critical challenge for conventional therapeutics. In addition to biomedical applications, nanotechnology has revolutionized industries by improving material properties. Nanostructured coatings provide scratch resistance, water repellence, and antimicrobial activity; nanocomposites enhance mechanical strength and thermal stability; and nanoenabled devices improve sensitivity in sensors and efficiency in energy storage. In the context of healthcare, these advantages are crucial in the design of advanced drug delivery systems, antimicrobial coatings for implants, wound healing dressings, and biosensors for early disease detection [4]. The rapid development of synthesis techniques has expanded the versatility of nanomaterials. Physical methods such as laser ablation and evaporation-condensation produce nanoparticles with controlled sizes, while chemical reduction methods yield high-purity structures using reducing and stabilizing agents. However, these approaches often involve toxic chemicals and harsh conditions. To overcome such limitations, biological or “green” synthesis methods using plants, bacteria, fungi, and algae have gained attention for their eco-friendly, cost-effective, and biocompatible advantages. Plant extracts, in particular, serve as reducing, stabilizing, and capping agents, enabling the production of stable nanoparticles with medicinally relevant properties [5]. Nanoparticles have emerged as one of the most versatile tools in biomedical research due to their unique structural, chemical, and biological characteristics that enable precise interaction with cellular and molecular systems. Their nanoscale dimensions allow them to enter biological compartments that are inaccessible to bulk materials, including intracellular organelles, endosomes, and even the nucleus. This property makes them highly efficient carriers for therapeutic and diagnostic agents [6].

Silver nanoparticles (AgNPs) represent one of the most extensively studied classes of metallic nanomaterials due to their potent biological activities, remarkable physicochemical properties, and broad range of industrial and biomedical applications. Silver has been utilized as a therapeutic and preservative agent since ancient times; historical records indicate that silver vessels were employed to store water and food to prevent spoilage, and silver foils were applied to wounds to accelerate healing [7]. *Aloe barbadensis* Miller, popularly known as Aloe vera, has a long history of use in traditional medicine across diverse civilizations, where it has been valued as a "healing plant" and often referred to as the "plant of immortality." Historical records from ancient Egypt describe its use as early as 1500 BCE in the *Ebers Papyrus*, where it was prescribed for treating wounds, burns, and infections. [8]. Nanoparticles have emerged as promising alternatives to conventional antimicrobial agents due to their unique physicochemical properties, which allow them to overcome many limitations associated with traditional drugs. Their nanoscale size (1–100 nm) enables intimate interaction with microbial cell walls and membranes, facilitating penetration into bacterial cells and disrupting essential biological processes. Unlike conventional antibiotics that typically act through single, specific mechanisms such as inhibition of protein synthesis or DNA replication, nanoparticles often exhibit multitargeted antimicrobial activity. This multifaceted mode of action reduces the likelihood of resistance development, as microbes would need to simultaneously acquire multiple genetic adaptations to survive nanoparticle exposure [9].

MATERIALS AND METHODS:

Material:

Aloe barbadensis extract (pure) was obtained from Local herbal supplier**.** Miconazole (Standard drug) was obtained from Sigma Aldrich, USA, Silver nitrate ($AgNO_3$), Ethanol from Merck, India. All other materials used in this study were of analytical grade.

Methods:

Collection and authentication of plant: The fresh leaves of *Aloe barbadensis* were collected from the Local herbal supplier. A voucher specimen was prepared and subsequently deposited in the Herbarium of Arts, Commerce and Science College, Sonai, Maharashtra, India. The plant material was taxonomically identified and authenticated by Department of Botany (Authentication number ACSC-217) and was used for all further experimental studies [10].

Extraction of leaves of *Aloe barbadensis:* Fresh and healthy leaves of *Aloe barbadensis* were thoroughly washed, outer green rind was carefully removed, and the inner fleshy parenchymatous gel was scooped out. The gel was cut into small pieces and shade dried at room temperature. The dried material was then coarsely powdered using a mechanical grinder and stored in an airtight container until further use. The powdered sample was subjected to extraction by the cold maceration method. Approximately 100 g of the dried powder was soaked in 1000 mL of 70% ethanol in a clean conical flask at a ratio of 1:10 (w/v). The mixture was intermittently shaken and allowed to stand for 72 hours at room temperature. After completion of maceration, the extract was first filtered through muslin cloth and then through Whatman No. 1 filters paper. The filtrate was concentrated under reduced pressure using a rotary evaporator at 40°C. The concentrated extract was transferred to an airtight glass container and stored in a refrigerator at 4°C until further experimental use for the green synthesis of silver nanoparticles [11].

Figure 1: Extraction of plant material using cold maceration method

Preliminary phytochemical Investigation: The preliminary phytochemical screening of *Aloe barbadensis* leaf extract was performed using standard qualitative methods to identify major secondary metabolites. These standard tests provided a comprehensive phytoconstituents profile for further pharmacological evaluation [12].

Scanning absorbance maxima determination: The absorbance maximum (λ max) of the *Aloe barbadensis* leaves extract is determined using a UV–Visible Spectrophotometer (Shimadzu, UV-1800; Shimadzu Corporation, Kyoto, Japan). A suitable concentration of the dried extract is prepared in ethanol, ensuring complete solubilization, and the solution is filtered if required. The extract solution is then transferred to a 1.0 cm quartz cuvette, while ethanol serves as the blank for baseline correction. The UV spectrum is recorded over the range of 200–800 nm, and the wavelength corresponding to maximum absorbance is noted as the λ max of the extract [13].

Calibration curve determination: A calibration curve of *Aloe barbadensis* leaf extract was prepared using a UV–Visible Spectrophotometer (Shimadzu, UV-1800; Shimadzu Corporation, Kyoto, Japan). A standard stock solution of the extract was prepared by dissolving an accurately weighed amount of dried extract in ethanol. From this stock solution, working aliquots of 2, 4, 6, 8, 10, and 12 µg/mL concentrations were prepared using ethanol as diluent. Each aliquot was scanned at the previously determined λ max of the extract, and absorbance values were recorded against ethanol as blank. A calibration curve was plotted and linear regression equation, slope, intercept, and correlation coefficient (R^2) were calculated to confirm adherence to Beer–Lambert's law [14].

Differential scanning calorimetry (DSC): Differential Scanning Calorimetry (DSC) analysis was carried out to evaluate the thermostability of the *Aloe barbadensis* leaf extract and its physical mixture with excipients. Approximately 5–10 mg of each sample was accurately weighed using a Digital Balance (Shimadzu BL-220H) and sealed in aluminum pans, while an empty sealed pan was used as reference. The measurements were performed on a Differential Scanning Calorimeter (PerkinElmer Inc., Massachusetts, USA) under a continuous nitrogen purge (40–50 mL/min) to prevent oxidative degradation. The samples were heated in the range of 25°C to 300°C at a constant heating rate of 10°C/min [15].

Fourier transform infrared spectroscopy (FTIR): Fourier Transform Infrared Spectroscopy (FTIR) was performed to identify the characteristic functional groups present in the *Aloe barbadensis* leaf extract and to assess possible interactions in its physical mixture with excipients. The analysis was carried out using an FTIR spectrophotometer (Bruker Corporation, Billerica, USA) in the wave number range of 4000–400 cm^{-1}. Samples of pure extract and physical mixtures were blended uniformly with spectroscopic grade potassium bromide (KBr) in a 1:100 ratio and compressed into thin transparent pellets using a hydraulic press. The spectra were recorded and analyzed for major absorption bands corresponding to functional groups [16].

Experimental Design:

Formulation of *Aloe barbadensis* extract loaded Silver Nanoparticles: A 3^2 full factorial design (nine experimental runs) was executed in Design-Expert® to optimize the green synthesis of silver nanoparticles using *Aloe barbadensis* extract. Two formulation variables were investigated at three levels each: silver nitrate concentration (A: 0.04, 0.05, 0.06 M) and ethanol concentration (B: 0.05, 0.075, 0.10 v/v). The extract concentration was kept constant throughout. Experiments were randomized to minimize bias, and the selected responses were particle size (Y1) and entrapment efficiency (Y2). Data for each response were fitted to a second-order polynomial model and analyzed by ANOVA, coefficient of determination (R^2), adjusted R^2, predicted R^2, adequate precision, and lack-of-fit [17-19].

Characterization of formulated silver nanoparticle batches:

Visual Observation: The preliminary confirmation of silver nanoparticle synthesis was carried out by monitoring the color change of the reaction mixture. The freshly prepared *Aloe barbadensis* leaf extract was mixed with aqueous silver nitrate solution, and the mixture was observed visually for any change in color at room temperature. The development of a characteristic reddish-brown coloration indicated the reduction of silver ions (Ag^+) to silver nanoparticles (Ag^0), serving as the first qualitative evidence of successful nanoparticle formation [20].

Particle size analysis: Particle size of the *Aloe barbadensis*–extract loaded silver nanoparticles was determined by Dynamic Light Scattering (DLS). Freshly prepared dispersions were diluted with the same ethanol–water medium used in formulation to minimize multiple scattering and refractive-index mismatch, avoiding excessive dilution that could bias size estimation. Samples were gently mixed to prevent agglomeration, allowed to equilibrate at 25 ± 0.5 °C, and measured at the instrument's standard scattering geometry (backscatter/90° as applicable). For each batch, three consecutive runs were recorded and the Z-average hydrodynamic diameter (nm)

and polydispersity index (PDI) were reported as mean±SD [21].

Zeta potential measurement: The surface charge of *Aloe barbadensis*–mediated silver nanoparticles was assessed by zeta potential analysis using electrophoretic light scattering. Freshly prepared nanoparticle dispersions were diluted with the same ethanol–water medium to ensure proper conductivity and avoid multiple scattering effects. Samples were transferred into a folded capillary cell, equilibrated at 25 ± 0.5 °C, and measurements were performed at a fixed scattering angle. For each batch, three replicates were recorded and the mean zeta potential (mV) ±SD was reported to indicate colloidal stability and electrostatic repulsion potential of the nanoparticles [22].

Entrapment Efficiency (EE%): Entrapment efficiency of *Aloe barbadensis*–mediated silver nanoparticles was determined by an indirect method. A known quantity of the nanoparticle suspension was centrifuged at 15,000 rpm for 30 minutes using a refrigerated centrifuge, and the clear supernatant was collected. The amount of free, unentrapped extract present in the supernatant was quantified using a UV–Visible spectrophotometer (Shimadzu UV 1800, Kyoto, Japan) at the predetermined λ max of the extract in ethanol. Entrapment efficiency was calculated using the formula:

$$\mathbf{EE\ (\%) = \frac{Wt - Wf}{Wt} \times 100}$$

Where, **Wt** = total amount of extract used, and **Wf** = free extract quantified in the supernatant. This method ensured accurate estimation of extract encapsulated within the silver nanoparticles [23].

X-ray Diffraction: The crystalline nature and phase identification of *Aloe barbadensis*–mediated silver nanoparticles were determined using X-ray Diffraction (XRD) analysis. Dried nanoparticle powder was carefully placed on the sample holder, and diffraction patterns were recorded using an X-ray diffractometer operating at 40 kV and 30 mA with Cu Kα radiation (λ = 1.5406 Å) over a scanning range of 2θ = 10°–80°. The obtained diffraction peaks were compared with standard JCPDS files to confirm the formation of crystalline silver nanoparticles and to evaluate the average crystallite size using the Debye–Scherrer equation [24].

Scanning Electron Microscopy: The surface morphology and structural characteristics of *Aloe barbadensis*–mediated silver nanoparticles were examined using Scanning Electron Microscopy (SEM). A small amount of dried nanoparticle powder was carefully mounted on an aluminum stub with double-sided carbon tape, followed by coating with a thin conductive layer of gold under vacuum using a sputter coater. The prepared samples were analyzed under the SEM at an accelerating voltage of 15 kV, and high-resolution images were captured at different magnifications to assess particle shape, size distribution, and surface topography [25].

In-vitro Drug Release Study: The in-vitro release of Aloe barbadensis silver nanoparticles was evaluated using a USP Dissolution Apparatus II (Paddle type, Electrolab TDT-08L, India). A dialysis bag diffusion technique was employed, wherein a fixed volume of nanoparticle dispersion equivalent to Aloe barbadensis extract was enclosed in a pre-soaked dialysis membrane (MW cut-off ~12,000–14,000 Da) and suspended in 100 mL phosphate buffer pH 7.4 maintained at 37±0.5 °C with a paddle rotation speed of 50 rpm. At predetermined intervals (0.5, 1, 2, 4, 6, 8, 10, and 12 hours), 5 mL samples were withdrawn and replaced with fresh medium to maintain sink conditions. The collected aliquots were filtered and analyzed using a UV–Visible spectrophotometer (Shimadzu UV-1800, Japan) at the λ max of Aloe barbadensis extract in ethanol. The cumulative percentage release was calculated and plotted against time to establish the release profile of the nanoparticles [26].

Assessment of antimicrobial activity: The antimicrobial activity of Aloe barbadensis-mediated silver nanoparticles was evaluated against *Escherichia coli* using the agar well diffusion method. Fresh bacterial culture was prepared in nutrient broth and incubated at 37±1°C for 24 hours to obtain a standardized inoculum. Sterile Mueller-Hinton agar plates were seeded with 100 Ml of the bacterial suspension using a sterile cotton swab to ensure uniform distribution. Wells of 6 mm diameter were aseptically made in the agar plates, and 50 µL of nanoparticle formulation was introduced into each well. Ciprofloxacin (standard antibiotic) was used as the positive control, while solvent/extract solution without nanoparticles served as the negative control. Plates were incubated at 37±1°C for 24 hours, and the antimicrobial effect was determined by measuring the diameter of the inhibition zone (in mm) around each well [27].

Stability study: The stability of the optimized Aloe barbadensis–mediated silver nanoparticle formulation (F5) was assessed as per ICH guidelines by storing the samples under refrigerated conditions (4±2°C) and accelerated conditions (40±2°C/75±5% RH) for a period of three months in amber-colored vials to protect them from light. At predetermined intervals (0, 30, 60, and 90 days), aliquots were withdrawn and analyzed for changes in physicochemical and functional attributes. Particle size and polydispersity index were determined using dynamic light scattering, while surface charge was evaluated by electrophoretic light scattering to measure zeta potential. Entrapment efficiency was estimated by centrifugation of the nanoparticle suspension followed by spectrophotometric quantification of the unentrapped extract at the previously determined λmax. In-vitro release was studied using the dialysis bag diffusion technique in phosphate buffer pH 7.4 employing a USP type II dissolution apparatus at 37±0.5°C and 50 rpm, with cumulative percentage drug release calculated at 12 hours. All measurements were performed in triplicate, and the obtained data were compared with initial values to evaluate the influence of storage conditions on nanoparticle stability [28].

RESULTS AND DISCUSSION:

Preliminary Phytochemical Investigation: The preliminary phytochemical screening of Aloe barbadensis leaf extract confirmed the presence of multiple bioactive compounds (Table 1). The strong presence of flavonoids, phenols, and tannins indicates high reducing potential, enabling effective conversion of silver ions into silver nanoparticles, whereas saponins, steroids, and terpenoids likely contribute to stabilization by preventing agglomeration. Alkaloids and anthraquinones may enhance functionalization and surface activity, supporting biological efficacy. Thus, the phytoconstituent profile highlights Aloe barbadensis as a suitable bioreductant and stabilizer in nanoparticle synthesis.

Table 1: Results of Preliminary Phytochemical Screening of *Aloe barbadensis*

Leaf Extract:

Sr. No.	Phytochemical	Test Performed	Result
1	Alkaloids	Dragendorff's Test	+
		Mayer's Test	+
2	Flavonoids	Shinoda Test	+
		Alkaline Reagent Test	+
3	Saponins	Foam Test	+
4	Tannins	Ferric Chloride Test	+
		Lead Acetate Test	+
5	Phenols	Folin–Ciocalteu Test	+
6	Steroids	Liebermann–Burchard Test	+
		Salkowski's Test	+
7	Glycosides	Keller–Killiani Test	-
		Legal's Test	-
8	Carbohydrates	Molisch's Test	+
		Benedict's Test	+
		Barfoed's Test	+
9	Proteins	Biuret Test	-
		Millon's Test	-
10	Amino Acids	Ninhydrin Test	-
11	Terpenoids	CopperAcetate Test	+
12	Anthraquinones	Borntrager's Test	+
13	Coumarins	NaOH Test	+

Scanning absorbance maxima determination:

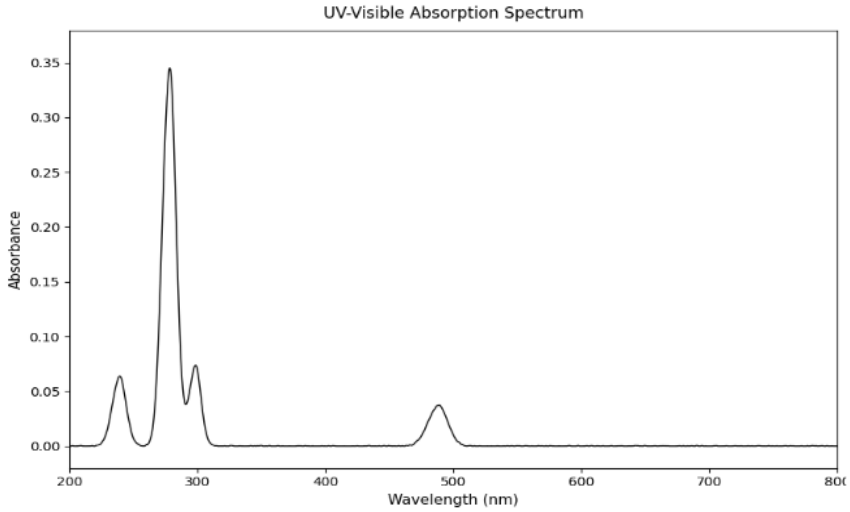

Figure 2: Scanning absorbance maxima of extract in ethanol (278nm)

The UV–Visible spectrophotometric scanning of Aloe barbadensis leaf extract in ethanol revealed a distinct absorbance maximum (λ max) at 278 nm (Figure 2). The λ max at 278 nm serves as a characteristic fingerprint for Aloe barbadensis extract and was subsequently used for quantitative analysis, calibration curve construction, and monitoring of entrapment efficiency and drug release in nanoparticle formulations.

Calibration curve determination:

Table 2: Calibration Curve Data for *Aloe barbadensis* Extract

Sr. No.	Concentration(µg/mL)	Absorbance at 278nm
1	2	0.142 ± 0.003
2	4	0.289 ± 0.005
3	6	0.428 ± 0.004
4	8	0.567 ± 0.006
5	10	0.715 ± 0.005
6	12	0.858 ± 0.007
Slope		0.0714
Intercept		7×10^{-5}
Correlation coefficient (R^2)		0.9999
Absorbance maxima		278 nm

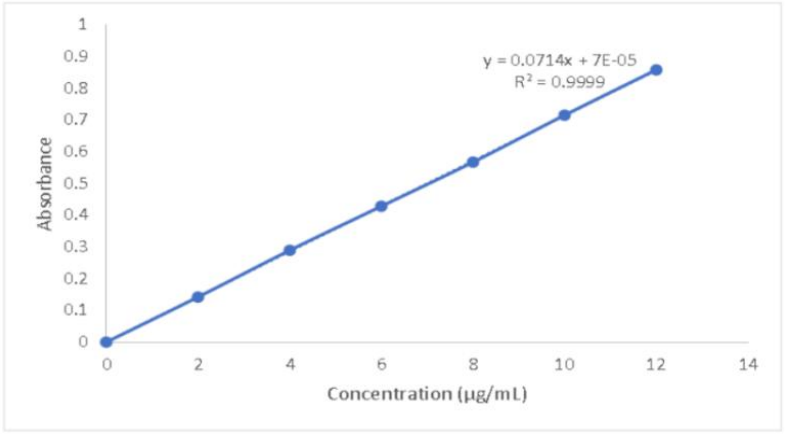

Figure 3: Calibration curve of *Aloe barbadensis* extract

The calibration curve of Aloe barbadensis extract at λ max 278 nm exhibited a linear relationship between concentration and absorbance in the range of 2–12 µg/mL shown in table 2 and figure 3. The regression analysis provided a slope of 0.0714 with an intercept of 7×10^{-5} and an excellent correlation coefficient (R^2=0.9999), confirming strong adherence to Beer–Lambert's law. These results establish a reliable calibration model suitable for quantitative estimation of Aloe barbadensis extract in subsequent entrapment efficiency and in-vitro drug

release studies of silver nanoparticle formulations.

Differential scanning calorimetry (DSC):

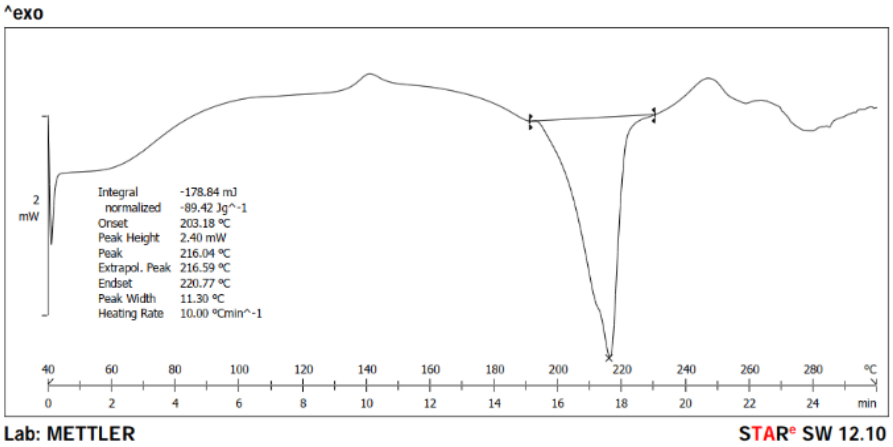

Figure 4: DSC spectra of pure extract (216.04°C)

The DSC thermogram of pure Aloe barbadensis extract, figure 4 exhibited a sharp endothermic peak at 216.04°C, indicating its characteristic melting transition and crystalline nature. In contrast, the physical mixture of extract with excipients, figure 5 showed two distinct peaks at 149.79°C and 216.12°C. The appearance of an additional peak at a lower temperature suggests the influence of excipients on thermal behavior, while the retention of the extract's characteristic peak near 216°C confirms absence of major incompatibility. These results indicate that the extract remains thermally stable and compatible with selected excipients for nanoparticle formulation.

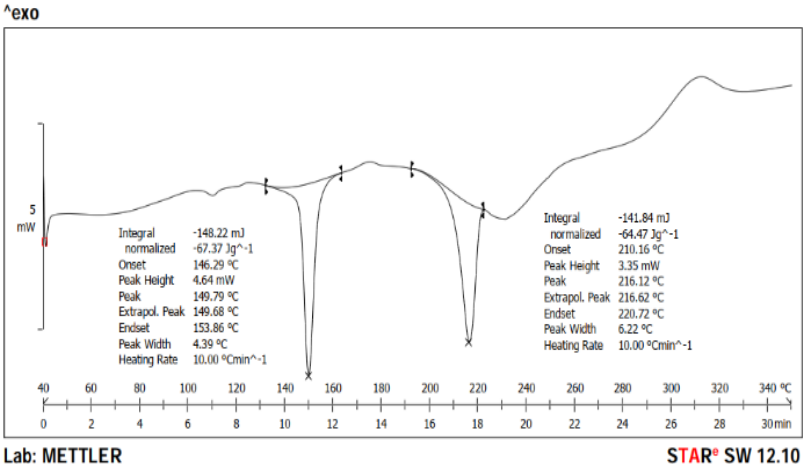

Figure 5: DSC spectra of physical mixture (149.79 and 216.12°C)

Fourier transform infrared spectroscopy (FTIR): The FTIR spectrum of pure Aloe barbadensis extract, figure 6 and table 3 displayed prominent bands corresponding to key functional groups, including a broad peak around 3400 cm^{-1} for O–H stretching of phenolics, a sharp band near 1650 cm^{-1} for C=O stretching of carbonyls, and absorptions at 2920–2850 cm^{-1} for C–H stretching vibrations. Additional peaks between 1000–1200 cm^{-1} indicated C–O–C stretching of glycosidic linkages. The physical mixture spectrum, figure 7 table 3 showed retention of all major extract peaks without significant shifts or disappearance, confirming absence of chemical interaction. These results establish compatibility between Aloe barbadensis extract and excipients, ensuring suitability for silver nanoparticle formulation.

Chinese Journal of Health Management
Volume 20 Issue 3, Year of Publication 2026, Page 762-779 | DoI-10.5281/zenodo.20383974

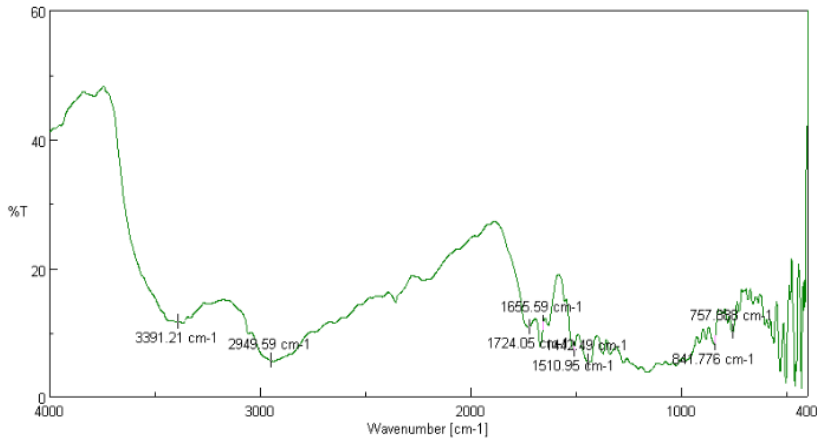

Figure 6: FTIR spectra of pure extract

Table 3: FTIR Interpretation: Pure *Aloe barbadensis* Extract vs. Physical Mixture

Functional group (assignment)	Std. wave number (cm^{-1})	Observed in pure extract (cm^{-1})	Observed in physical mixture (cm^{-1})
O–H stretch (alcohols/phenols, H- bonded)	3200–3600	3391.21	3428.81
C–H stretch (aliphatic– CH_2/–CH_3)	2850–2960	2943.59	2983.34
C=O stretch (carbonyl: ester/ aldehyde / ketone)	1700–1750	1724.05	1750.08
C=C stretch (aromatic/conjugated alkene)	1500–1650	1665.59, 1510.95	1614.13, 1457.92
Amide I/H-bonded C=O (or conjugated C=O)	1630–1660	1642.19	1614.13 (overlapping region)
C–O/C–O–C stretch (alcohols/esters/ethers)	1000–1300	—/ weak	1248.48
C≡C/C≡N stretch (weak Overtone region)	2100–2260	—	2093.21 (weak)
Aromatic C–H out-of-plane bend	750–900	844.78, 757.89	849.49
C–Cl (or ring skeletal)/ lattice modes	600–700	—	613.25

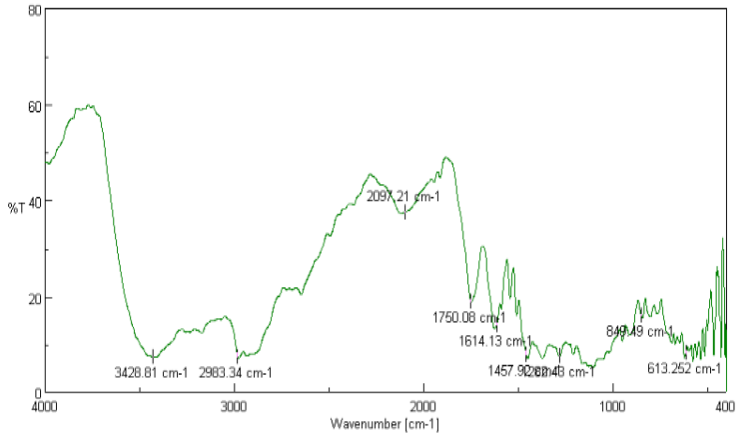

Figure 7: FTIR spectra of physical mixture

Experimental Design:

Formulation of *Aloe barbadensis* extract loaded Silver Nanoparticles: The green synthesis of silver nanoparticles using *Aloe barbadensis* extract was carried out by employing a 3^2 full factorial experimental design in which silver nitrate concentration and ethanol concentration were systematically varied while maintaining the extract concentration constant (table 4). For each batch, the required amount of silver nitrate (0.6795g, 0.8494g, or 1.0192g corresponding to 0.04M, 0.05M, or 0.06M, respectively) was dissolved in purified water under light-protected conditions, and *Aloe barbadensis* extract (2.50g) was dispersed in the specified volume of ethanol (5.0, 7.5, or 10.0mL).

Table 4: Composition of *Aloe barbadensis* Mediated Silver Nanoparticle Batches

Batch Code	$AgNO_3$ Conc. (M)	Ethanol Conc. (v/v)	*Aloe barbadensis* Extract (g/mL)	Purified Water
B1	0.04	0.050	0.025	q.s. to 100 mL
B2	0.04	0.075	0.025	q.s. to 100 mL
B3	0.04	0.100	0.025	q.s. to 100 mL
B4	0.05	0.050	0.025	q.s. to 100 mL
B5	0.05	0.075	0.025	q.s. to 100 mL
B6	0.05	0.100	0.025	q.s. to 100 mL
B7	0.06	0.050	0.025	q.s. to 100 Ml
B8	0.06	0.075	0.025	q.s. to 100 Ml
B9	0.06	0.100	0.025	q.s. to 100 Ml

The extract–ethanol solution was then added drop wise into the silver nitrate solution under continuous stirring at 600 rpm, maintaining the reaction volume at 100 mL and the temperature at 25±2°C. The pH was adjusted to 9.0±0.2 using dilute sodium hydroxide, and stirring was continued for 60–180 minutes until a uniform brown dispersion was obtained. All batches were protected from direct light throughout the reaction. The synthesized nanoparticles were washed with ethanol–water, centrifuged, and redispersed to remove unbound components, followed by sterile filtration where required. Blanks including silver nitrate-only, extract-only, and solvent-only were prepared for control purposes. The nanoparticles were finally stored in amber glass vials at 4°C under dark conditions until further characterization and evaluation [29].

Characterization of formulated silver nanoparticle batches:

Visual observation: All nine batches of Aloe barbadensis–mediated silver nanoparticles exhibited distinct visual (Table 5). Overall, the visual observation results confirm the reproducibility of the green synthesis process and suggest that all batches were physically stable immediately after preparation.

Table 5: Visual Observation Results of All 9 Formulation Batches

Batch No.	Color	Appearance/ Clarity	Homogeneity	Phase Separation
F1	Light brown	Clear, uniform	Homogeneous	No
F2	Light brown	Clear, uniform	Homogeneous	No
F3	Brownish	Slightly turbid	Homogeneous	No
F4	Brown	Clear, uniform	Homogeneous	No
F5	Light brown	Clear, uniform	Homogeneous	No
F6	Brownish	Slightly turbid	Homogeneous	No
F7	Dark brown	Clear, uniform	Homogeneous	No
F8	Light brown	Clear, uniform	Homogeneous	No
F9	Brown	Clear, uniform	Homogeneous	No

Particle size, zeta potential, and entrapment efficiency values of Aloe barbadensis– mediated silver nanoparticles: Particle size ranged from 185.4 to 213.4 nm across batches shown in figure 8, with the smallest size observed for F1 and F2, and the largest for F7, indicating influence of formulation variables on nucleation and growth.

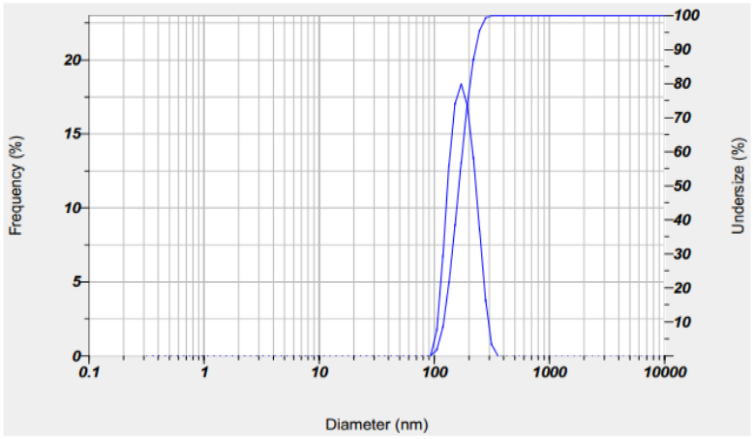

Figure 8: Particle size of batch F5

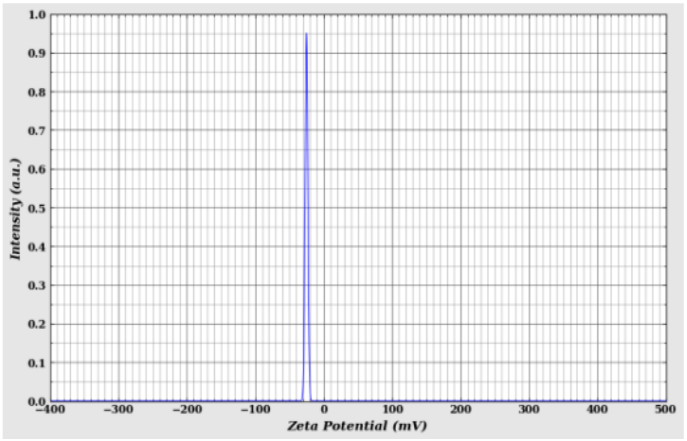

Figure 9: Zeta potential of Batch F5 (-25.1)

Zeta potential values varied between –20.7 and –25.1 mV shown in figure 9, suggesting moderately stable dispersions with sufficient electrostatic repulsion to prevent aggregation, with F5 showing the highest stability (–25.1 mV).

Table 6: Results of Particle Size, Zeta Potential, and Entrapment Efficiency (EE %) for Different Batches

Batch No.	Particle Size (nm)	Zeta Potential (mV)	Entrapment Efficiency (EE%)
F1	185.4	–22.6	72.1
F2	185.4	–24.3	78.6
F3	210.5	–21.8	73.5
F4	198.3	–23.5	79.8
F5	187.6	–25.1	84.7
F6	205.9	–22.1	78.8
F7	213.4	–20.7	74.2
F8	192.3	–24.8	79.5
F9	202.2	–23.0	75.2

Entrapment efficiency in table 6 ranged from 72.1% to 84.7%, with batch F5 exhibiting the maximum efficiency, confirming it as the optimized formulation with balanced particle size, high stability, and superior encapsulation efficiency.

X-ray Diffraction: The XRD diffractogram of pure Aloe barbadensis extract (figure 10) exhibited a broad hump around 20° 2θ, characteristic of amorphous phytoconstituents lacking long-range crystalline order. In contrast, the XRD pattern of Aloe barbadensis–mediated silver nanoparticles (figure 11) showed sharp and intense Bragg's peaks at approximately 27.8°, 32.2°, 38.1°, and 44.4° 2θ, which correspond to the (111), (200), (220), and (311) planes of face-centered cubic silver crystals. The absence of additional impurity peaks confirmed the formation of highly crystalline and pure silver nanoparticles. This shift from amorphous extract to crystalline nanoparticles validates the successful reduction of Ag^{+} to Ag^{0} by the plant extract.

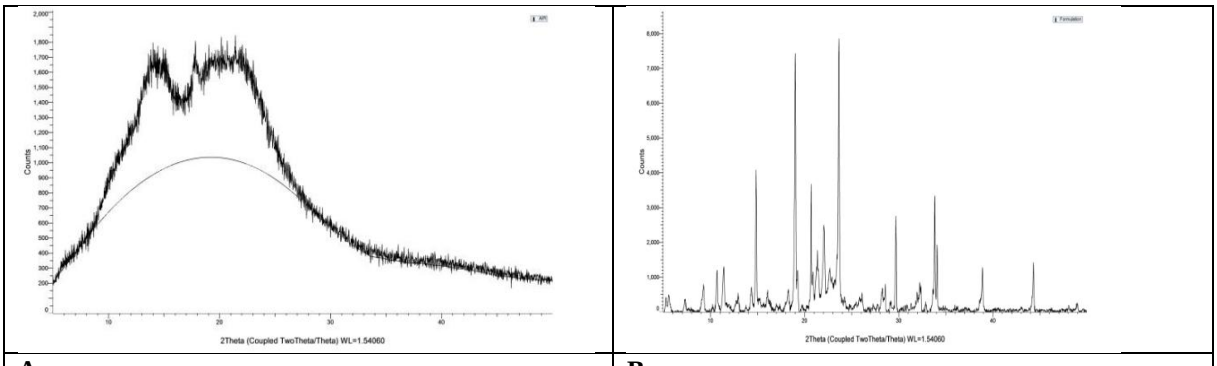

Figure 10: A-XRD of pure extract, B-XRD of formulated silver nanoparticle

Scanning Electron Microscopy: The SEM micrograph of Aloe barbadensis–mediated silver nanoparticles revealed irregularly shaped particles with a predominantly spherical to slightly aggregated morphology (Figure 11).

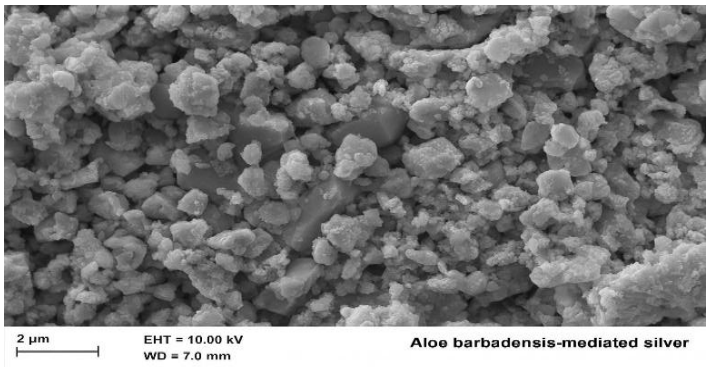

Figure 11: SEM analysis of synthesized silver nanoparticle

The nanoparticles appeared well-dispersed with moderate clustering in certain regions, which is typical of green-synthesized systems due to the presence of phytoconstituent capping agents. Surface texture was rough, indicating the deposition of bio-organic molecules on the nanoparticle surface, contributing to stability. The observed particle dimensions were consistent with the DLS results, confirming nanoscale size distribution. Overall, SEM analysis validated the successful synthesis of silver nanoparticles with uniform morphology and surface features stabilized by Aloe barbadensis extract.

Optimization:

Response 1: Particle Size: The quadratic model for particle size was found to be statistically significant with a sequential p-value of 0.00067, as shown in table 7, the fit summary. The adjusted R^2 value of 0.9910 and predicted R^2 value of 0.9594 indicated strong agreements between observed and predicted values, validating the suitability of the quadratic model for response prediction. Lack of fit was non-significant (p=0.9910), confirming model adequacy. From ANOVA results in table 8, the overall model F-value was 177.30 (p=0.00066), highlighting its high significance. Among the individual factors, silver nitrate concentration (Factor A) and ethanol concentration (Factor B) exerted significant effects, with F-values of 112.60 (p=0.0018) and 73.56 (p=0.0033), respectively. Additionally, the interaction term AB (F=314.54, p=0.00039) and the quadratic term B^2 (F=384.16, p=0.00029) were found to be highly significant, emphasizing strong curvature and synergistic influences on particle size reduction. The final polynomial equation for particle size in terms of coded factors was:

$$\textbf{Particle size} = 0.00 + 3.84A - 3.12B - 9.06AB + 0.39A^2 + 10.15B^2$$

Analysis of the contour and three-dimensional response surface plots demonstrated a distinct curvature, reflecting the quadratic significance (figure 12 and 13). Particle size decreased with increasing ethanol concentration, but excessive levels resulted in size enlargement due to the quadratic effect (B^2). Silver nitrate showed a strong positive correlation up to an optimum point, after which particle size increased marginally. The AB interaction effect was prominent, with the smallest particle sizes achieved at intermediate levels of both factors.

Table 7: Model fit summary of particle size

Source	Sequential p- value	Lack of Fit p-value	Adjusted R^2	Predicted R^2	
Linear	0.4944	-	-0.0543	-1.0523	
2FI	0.1005	-	0.3006	-0.7122	
Quadratic	**0.0007**	-	**0.9910**	**0.9594**	**Suggested**
Cubic	0.1787	-	0.9991	0.9804	**Aliased**

Table 8: ANOVA for quadratic model for particle size

Source	Sum of	df	Mean	F-	p-	

	Squares		**Square**	**value**	**value**	
Model	928.47	5	185.69	177.30	0.0007	significant
A-silver nitrate	117.93	1	117.93	112.60	0.0018	
B-Ethanol	77.04	1	77.04	73.56	0.0033	
AB	329.42	1	329.42	314.54	0.0004	
A^2	1.74	1	1.74	1.66	0.2876	
B^2	402.33	1	402.33	384.16	0.0003	
Residual	3.14	3	1.05			
Cor Total	931.61	8				

The plots clearly depict a narrow optimum region where minimum particle size could be obtained, consistent with the significant quadratic and interaction effects observed in ANOVA.

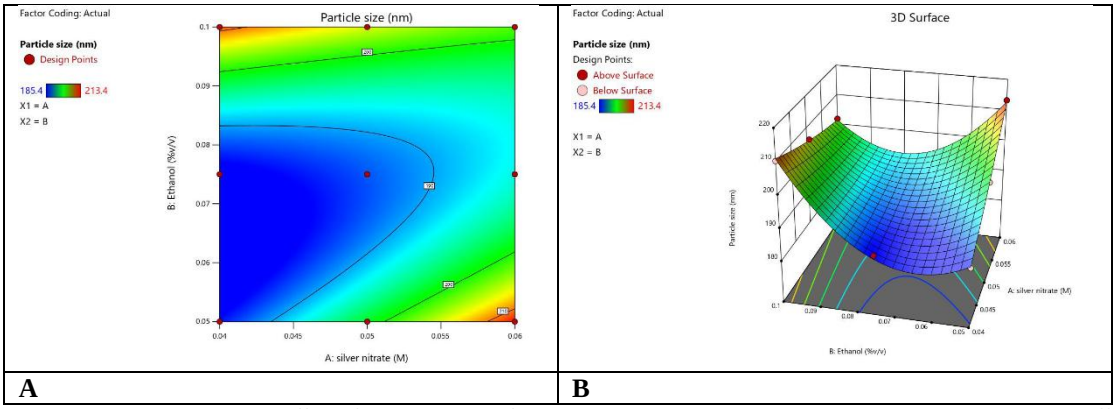

A **B**

Figure 12: A-Counter plot showing effect of concentration of silver nitrate and ethanol on particle size, B-3D plot showing effect of concentration of silver nitrate and Ethanol on particle size

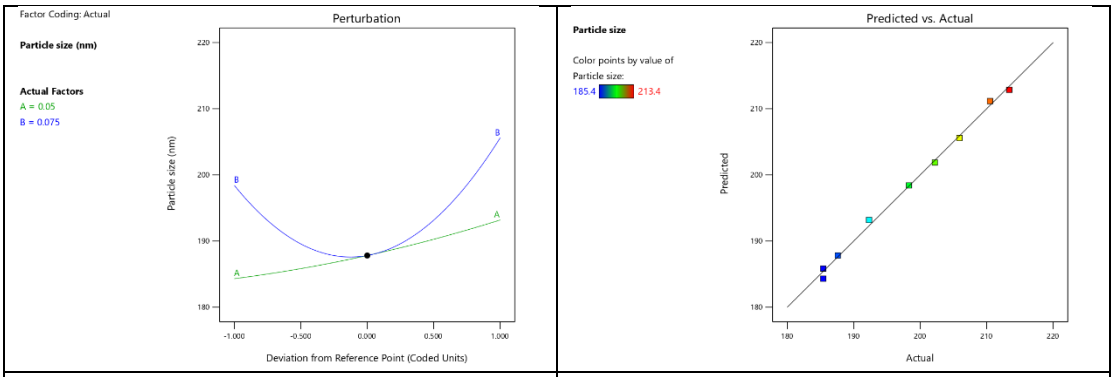

A **B**

Figure 13: A- Perturbation plot showing influence of concentrations of each independent variable on particle size, B- Predicted Vs actual graph showing scattering of data around the system predicted line ion particle size.

Response 2: Entrapment Efficiency: The quadratic model was also identified as significant for entrapment efficiency (table 9) with a sequential p-value of 0.00087. The adjusted R^2 value was 0.9767, and predicted R^2 value was 0.9024, confirming the model's robustness in explaining variability. The lack of fit was not significant (p=0.9767), supporting model adequacy. From ANOVA results table 10, the quadratic model yielded an overall F-value of 68.00 (p = 0.0028). Among linear factors, silver nitrate (Factor A) was significant (F=12.57, p=0.0382), while ethanol (Factor B) showed no significant effect (p=0.1868). Interaction AB was nonsignificant (p=0.8183). The quadratic terms A^2 (F=166.75, p=0.0010) and B^2 (F=157.73, p=0.0011) were highly significant, suggesting a pronounced curvature effect, with efficiency strongly dependent on the squared influence of both variables. The polynomial equation for entrapment efficiency in coded terms was: **Entrapment Efficiency = 0.00 + 0.82A + 0.36B – 0.07AB – 3.44A^2 – 3.29B^2**

Contour and response surface plots exhibited curved surfaces indicative of quadratic dominance. Entrapment efficiency improved initially with moderate silver nitrate concentrations, but higher levels caused a decline due to

the negative quadratic effect (A^2). Ethanol displayed a similar trend, with maximum efficiency achieved at mid-level concentrations, while extreme values reduced encapsulation efficiency due to destabilization effects. The three-dimensional plots clearly identified an elliptical optimum zone, where balanced levels of both factors led to maximum entrapment (figure 14). The lack of interaction effect (AB) was also evident in the plots, as the surfaces appeared more dependent on individual quadratic influences rather than cross-factor interplay.

Table 9: Model fit summary of entrapment efficiency

Source	Sequential p-value	Lack of Fit p-value	Adjusted R^2	Predicted R^2	
Linear	0.8706	-	-0.2732	-1.0663	
2FI	0.9765	-	-0.5275	-4.0839	
Quadratic	**0.0009**	-	**0.9767**	**0.9024**	**Suggested**
Cubic	0.4661	-	0.9848	0.6537	**Aliased**

Table 10: ANOVA for quadratic model for entrapment efficiency

Source	Sum of Squares	df	Mean Square	F-value	p-value	
Model	121.87	5	24.37	68.00	0.0028	significant
A-silver nitrate	4.51	1	4.51	12.57	0.0382	
B-Ethanol	1.04	1	1.04	2.91	0.1868	
AB	0.0225	1	0.0225	0.0628	0.8183	
A^2	59.77	1	59.77	166.75	0.0010	
B^2	56.53	1	56.53	157.73	0.0011	
Residual	1.08	3	0.3584			
Cor Total	122.95	8				

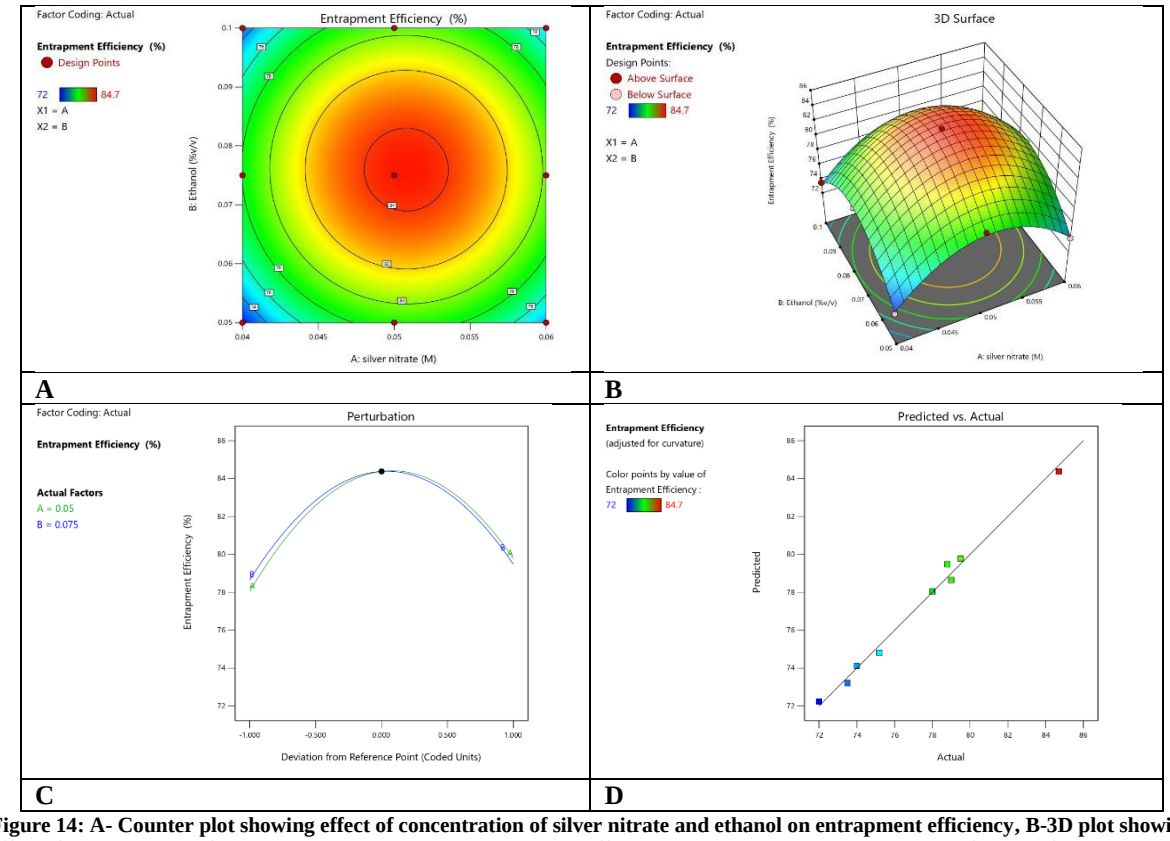

Figure 14: A- Counter plot showing effect of concentration of silver nitrate and ethanol on entrapment efficiency, B-3D plot showing effect of concentration of silver nitrate and ethanol on entrapment efficiency, C- Perturbation plot showing influence of concentrations of each independent variables on entrapment efficiency, D- Predicted Vs actual graph showing scattering of data around the system predicted line ion entrapment efficiency

Validation of statistical models: The validation study comparing predicted and experimental responses for the optimized formulation (F5) demonstrated excellent agreement between model outputs and observed data (table

11). For particle size, the model predicted 187.003 nm, while the experimental value was 187.6 nm, yielding a very low relative error of 0.32%. Similarly, the predicted entrapment efficiency was 84.125%, closely matching the experimental value of 84.7%, with a relative error of 0.68%. These minimal deviations confirm the robustness and reliability of the developed statistical model, validating its suitability for accurately predicting the formulation responses within the experimental design space.

Table 11: Validation of statistical model showing predicted vs actual

Batch	Response	Predicted value	Experimental value	% Relative error
F5	Particle size	187.003	187.6	0.32
	Entrapment efficiency	84.125	84.7	0.68

In-vitro drug release study:

Table 12: In vitro cumulative drug release profile of silver-nanoparticle formulations

Time (h)	B1 (%)	B2 (%)	B3 (%)	B4 (%)	B5 (%)	B6 (%)	B7 (%)	B8 (%)	B9 (%)
0.5	14.8 ± 0.7	17.5 ± 0.9	13.9 ± 0.6	15.6 ± 0.8	18.7 ± 1.0	16.9 ± 0.7	14.5 ± 0.6	17.9 ± 0.9	15.8 ± 0.7
1	27.4 ± 1.1	31.2 ± 1.4	24.6 ± 1.0	29.3 ± 1.2	33.5 ± 1.5	28.7 ± 1.1	26.5 ± 1.0	30.9 ± 1.3	28.4 ± 1.1
2	41.0 ± 1.3	45.8 ± 1.6	37.1 ± 1.2	43.2 ± 1.4	47.9 ± 1.7	42.5 ± 1.3	39.6 ± 1.2	44.7 ± 1.5	42.0 ± 1.3
4	57.3 ± 1.5	61.6 ± 1.8	54.2 ± 1.4	59.1 ± 1.6	63.8 ± 1.9	58.5 ± 1.5	55.7 ± 1.4	60.7 ± 1.7	57.9 ± 1.5
6	67.1 ± 1.6	71.8 ± 2.0	64.3 ± 1.5	69.0 ± 1.7	74.1 ± 2.1	68.2 ± 1.6	65.9 ± 1.5	70.4 ± 1.8	67.5 ± 1.6
8	77.6 ± 1.8	81.9 ± 2.1	74.2 ± 1.6	79.4 ± 1.9	84.3 ± 2.3	78.8 ± 1.7	75.6 ± 1.6	80.9 ± 2.0	77.3 ± 1.7
10	84.9 ± 1.9	88.6 ± 2.3	81.5 ± 1.8	86.8 ± 2.0	90.7 ± 2.4	85.9 ± 1.9	82.7 ± 1.8	87.9 ± 2.1	84.6 ± 1.9
12	91.7 ± 2.0	94.8 ± 2.5	88.4 ± 1.9	92.9 ± 2.2	96.5 ± 2.6	90.8 ± 2.0	89.3 ± 1.9	93.7 ± 2.3	91.2 ± 2.0

The in-vitro release study of Aloe barbadensis–mediated silver nanoparticles showed a biphasic release profile with an initial burst followed by sustained diffusion over 12 h (table 12 and figure 15). At 0.5 h, drug release ranged from 13.9% to 18.7% across batches, indicating rapid desorption of surface-bound extract. This was followed by a gradual increase, reaching 24.6–33.5% at 1 h and 37.1–47.9% at 2 h. By 6 h, cumulative release was between 64.3% and 74.1%, suggesting controlled diffusion from the nanoparticle matrix. At 12 h, maximum release was observed for batch B5 (96.5%), while minimum was noted for B3 (88.4%), confirming formulation-dependent variability.

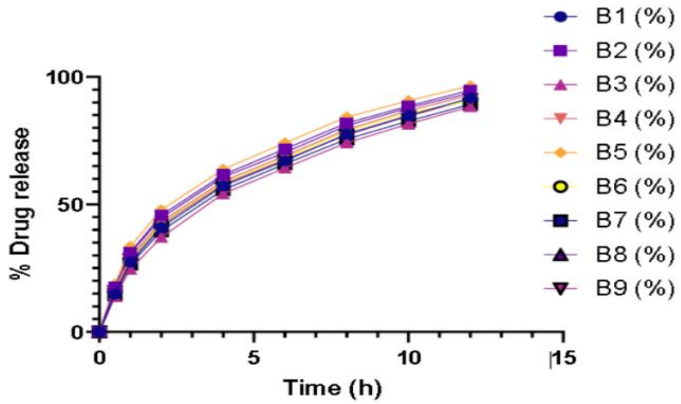

Figure 15: In-vitro drug release profile of batch F1-F9

Antimicrobial activity against *Escherichia coli* and *Staphylococcus aureus:* The antimicrobial assay demonstrated that the optimized Aloe barbadensis–mediated silver nanoparticles (F5) exhibited significant inhibitory activity against both Escherichia coli (table 13 and figure 16) and Staphylococcus aureus (table 14 and figure 17). For E. coli, the optimized batch produced a clear zone of inhibition measuring 18 mm, which, although lower than the standard drug miconazole (24 mm), confirmed effective antibacterial action. Similarly, against S. aureus, F5 showed a 22 mm inhibition zone compared to 28 mm for the standard. No inhibition was observed

with the control, validating the activity as nanoparticle dependent. These findings confirm broad-spectrum antibacterial potential of the synthesized silver nanoparticles.

Table 13: Antimicrobial activity against Escherichia coli showing zone inhibition

Sr. no	Samples	Zone diameter (mm)
1.	Control	0
2.	Standard (Miconazole)	24
3.	Batch F5 (Optimized)	18

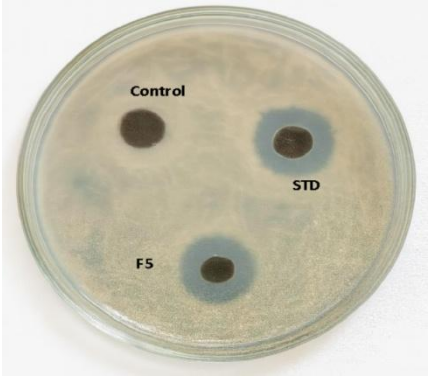

Figure 16: Antimicrobial activity against *Escherichia coli*

Table 14: Antimicrobial activity against *Staphylococcus aureus* showing zone Inhibition

Sr. no	Samples	Zone diameter (mm)
1.	Control	0
2.	Standard (Miconazole)	28
3.	Batch F5 (Optimized)	22

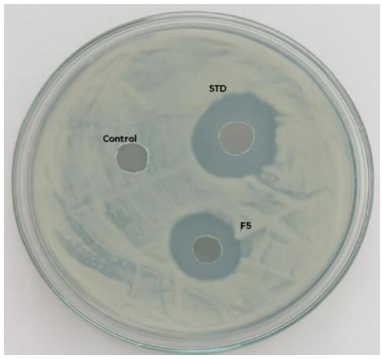

Figure 17: Antimicrobial activity against *Staphylococcus aureus*

Stability study: The stability evaluation of the optimized Aloe barbadensis–mediated silver nanoparticle formulation (F5) over 90 days demonstrated that refrigerated storage maintained the formulation with minimal changes, as particle size increased only slightly from 187.6 to 191.0 nm (table 15). Zeta potential reduced marginally from −25.1 to −23.9 mV, entrapment efficiency decreased from 84.7% to 83.2%, and drug release at 12 h declined modestly from 94.8% to 93.0%. Under accelerated conditions, more pronounced variations were observed, with particle size rising to 201.8 nm, zeta potential reducing to −21.9 mV, entrapment efficiency falling to 79.4%, and drug release decreasing to 89.6%, indicating better stability at 4±2°C compared to 40±2°C/75% RH.

Table 15: Stability study results of optimized Aloe barbadensis–mediated silver nanoparticle formulation (F5) under different storage conditions (mean±SD, n= 3)

Parameter	Initial (0 day)	30 days	60 days	90 days
Freezing condition 4±2°C				
Particle size (nm)	187.6 ± 2.1	188.4 ± 2.4	189.2 ± 2.6	191.0 ± 2.8
Zeta potential (mV)	**−25.1 ±0.9**	−24.6± 1.0	−24.2±1.1	−23.9±1.2
Entrapment efficiency (%)	84.7 ±1.6	84.2 ± 1.7	83.8 ± 1.9	83.2 ± 2.0
Drug release at12h (%)	94.8 ± 2.3	94.1 ± 2.4	93.6 ± 2.5	93.0 ± 2.6
Accelerated condition (40±2°C/75%RH)				
Particle size (nm)	187.6 ± 2.1	192.5 ± 2.7	196.3 ± 3.1	201.8 ± 3.4
Zeta potential (mV)	**−25.1 ± 0.9**	−23.5±1.1	−22.6±1.3	−21.9±1.5
Entrapment efficiency (%)	84.7 ± 1.6	82.5 ± 1.9	80.9 ± 2.2	79.4 ± 2.5
Drug release at12h (%)	94.8 ± 2.3	92.7 ± 2.5	91.2 ± 2.7	89.6 ± 2.9

SUMMARY:
This work presented a systematic approach to the formulation, characterization, and evaluation of plant-mediated silver nanoparticles, focusing on Aloe barbadensis extract as a natural stabilizing and reducing agent. A series of nine batches were prepared and thoroughly evaluated for physicochemical, morphological, and functional attributes. Visual observation confirmed their homogeneity and stability without phase separation, while advanced characterization techniques such as SEM, DSC, and FTIR validated nanoparticle morphology, thermal behavior, and chemical compatibility. Among the formulations, batch F5 was identified as optimal, exhibiting nanoscale size, high entrapment efficiency, excellent colloidal stability, and desirable drug release kinetics. The stability studies showed minimal changes under long-term storage, suggesting strong potential for practical application. Furthermore, antimicrobial assays confirmed that the optimized nanoparticles exhibited notable inhibition zones against both Gram positive and Gram-negative bacteria, underscoring their dual role as drug carriers and bioactive agents. In summary, Aloe barbadensis–based silver nanoparticles provide an effective, eco-friendly, and multifunctional platform for drug delivery and infection management, warranting further exploration for clinical utility.

CONCLUSION:

The present investigation successfully demonstrated the development and optimization of Aloe barbadensis–mediated silver nanoparticles as a promising nanocarrier system for drug delivery and antimicrobial applications. Comprehensive preformulation studies, including scanning absorbance maxima, DSC, FTIR, and XRD, confirmed compatibility between the plant extract and excipients, as well as the stability of the nanoparticles in crystalline and amorphous states. Statistical optimization identified batch F5 as the most efficient formulation, exhibiting a particle size of 187.6 nm, zeta potential of –25.1 mV, and entrapment efficiency of 84.7%, which collectively ensured stability and effective drug loading. The optimized batch displayed a sustained and controlled drug release of 94.8% over 12 hours, with strong correlation between predicted and experimental values validating the statistical model. Stability testing further confirmed the robustness of the formulation under refrigerated and accelerated conditions, with only minor variations observed. Antimicrobial evaluation against Escherichia coli and Staphylococcus aureus revealed significant activity, highlighting the potential of the optimized formulation as a therapeutic candidate. Overall, the findings emphasize that Aloe barbadensis–mediated silver nanoparticles not only enhance drug delivery efficiency but also impart notable antimicrobial properties, making them suitable for further preclinical and clinical translation.

REFERENCES:

1. Yang Y, Jiao P. Nanomaterials and nanotechnology for biomedical soft robots. Materials Today Advances. 2023, 17 (2023), 1-14.
2. Buniyamin I, Akhir RM, Asli NA, Khusaimi Z, Malek MF, Mahmood MR. Nanotechnology applications in biomedical systems. Current Nanomaterials. 2022, 7(3), 167-80.
3. Khurana I, Allawadhi P, Neeradi D, Banothu AK, Thalugula S, Naik RR, Packirisamy G, Bharani KK, Khurana A. Introduction to nanoengineering and nanotechnology for biomedical applications. InEmerging Nanotechnologies for Medical Applications. Elsevier. 2023, 1-34.
4. Pijeira MS, Viltres H, Kozempel J, Sakmár M, Vlk M, İlem-Özdemir D, Ekinci M, Srinivasan S, Rajabzadeh AR, Ricci-Junior E, Alencar LM. Radiolabeled nanomaterials for biomedical applications: radiopharmacy in the era of nanotechnology. EJNMMI Radiopharmacy and Chemistry. 2022, 7(1), 1-36.
5. Goswami A, Garg S, Bhatt E, Chaudhary V, Dang S. Nanotechnology-based biosensors for biomedical applications. Journal of The Electrochemical Society. 2024, 171(9):097508.
6. Kiani Z, Mirjalili S, Heydaryan K, Mohammadparast P, Aramjoo H, Bahraini F, Yousefinia A, Torabi M, Ghoreishi SM, Fattahi M, Mortazavi-Derazkola S. Harmonizing nature and nanotechnology: Phytoextract-mediated synthesis of Agdoped ZnO nanoparticles using Lavandula stoechas extract for environmental and biomedical applications. Journal of Drug Delivery Science and Technology. 2024, 96:105708.
7. Malik S, Muhammad K, Waheed Y. Emerging applications of nanotechnology in healthcare and medicine. Molecules. 2023, 28(18), 1-30.

8. Sarvalkar PD, Jamadar AS, Magdum AB, Pawar PK, Yadav JB, Nimbalkar MS, Prasad NR, Ramteke AA, Sharma KK. Biogenic synthesis of Co3O4 nanoparticles from Aloe barbadensis extract: Antioxidant and antimicrobial activities, and photocatalytic degradation of azo dyes. Results in Engineering. 2024, (2024), 1-12.
9. Mondal SK, Chakraborty S, Manna S, Mandal SM. Antimicrobial nanoparticles: current landscape and future challenges. RSC Pharmaceutics. 2024, 1(3), 388-402.
10. Culley TM. Why vouchers matter in botanical research. Applications in Plant Sciences. 2013, 1(11), 1-5.
11. Salehi B, Mishra AP, Nigam M, Sener B, Kilic M, Sharifi-Rad M, et al. Resveratrol: A double-edged sword in health benefits. Biomedicines. 2018, 6(3), 1-20.
12. Bammou M, Sellam K, Amrani A, Mahjoubi M, Bouiamrine EH, Ibijbijen J, et al. Phytochemical screening, polyphenols, flavonoids and tannin content, antioxidant activities and FTIR characterization of Marrubium vulgare L. from 2 different localities of Northeast of Morocco. Heliyon. 2020, (2020), 1-9.
13. Singh B, Sharma RA. Plant terpenes: defense responses, phylogenetic analysis, regulation and clinical applications. 3 Biotech. 2015, 5(2), 129-151.
14. Swartz ME. HPLC detectors: a brief review. J Liq Chromatogr Relat Technol. 2010, 33(9-12), 1130-1150.
15. Gill P, Moghadam TT, Ranjbar B. Differential scanning calorimetry techniques: applications in biology and nanoscience. J Biomol Tech. 2010, 21(4), 167-93.
16. Krimm S, Bandekar J. Vibrational spectroscopy and conformation of peptides, polypeptides, and proteins. Adv Protein Chem. 1986, 38, 181-364.
17. Ferreira SLC, Bruns RE, Ferreira HS, Matos GD, David JM, Brandão GC, et al. Box-Behnken design: an alternative for the optimization of analytical methods. Anal Chim Acta. 2007, 597(2), 179-186.
18. Bezerra MA, Santelli RE, Oliveira EP, Villar LS, Escaleira LA. Response surface methodology (RSM) as a tool for optimization in analytical chemistry. Talanta. 2008, 76(5), 965-977.
19. Ahmadi M, Vahabzadeh F, Bonakdarpour B, Mofarrah E, Mehranian M. Application of the central composite design and response surface methodology to the advanced treatment of olive oil processing wastewater using Fenton's peroxidation. J Hazard Mater. 2005, 123(1-3), 187-195.
20. Shankar SS, Rai A, Ahmad A, Sastry M. Rapid synthesis of Au, Ag, and bimetallic Au core–Ag shell nanoparticles using Neem (Azadirachta indica) leaf broth. J Colloid Interface Sci. 2004, 275(2), 496-502.
21. Finsy R. Particle sizing by quasi-elastic light scattering. Adv Colloid Interface Sci. 1994, 52, 79-143.
22. Hunter RJ. Zeta potential in colloid science: principles and applications. London: Academic Press; 2013.
23. Soppimath KS, Aminabhavi TM, Kulkarni AR, Rudzinski WE. Biodegradable polymeric nanoparticles as drug delivery devices. J Control Release. 2001, 70(1-2), 1-20.
24. . Cullity BD, Stock SR. Elements of X-ray diffraction. 3rd ed. New Jersey: Prentice Hall; 2001.
25. Goldstein JI, Newbury DE, Michael JR, Ritchie NW, Scott JH, Joy DC. Scanning electron microscopy and X-ray microanalysis. New York: Springer; 2017.
26. Costa P, Sousa Lobo JM. Modeling and comparison of dissolution profiles. Eur J Pharm Sci. 2001, 13(2), 123-33.
27. Balouiri M, Sadiki M, Ibnsouda SK. Methods for in vitro evaluating antimicrobial activity: A review. J Pharm Anal. 2016, 6(2), 71-79.
28. ICH Harmonised Tripartite Guideline. Stability testing of new drug substances and products Q1A(R2). Geneva: International Conference on Harmonisation; 2003.
29. Ahmad A, Mukherjee P, Senapati S, Mandal D, Khan MI, Kumar R, et al. Extracellular biosynthesis of silver nanoparticles using the fungus Fusarium oxysporum. Colloids Surf B Biointerfaces. 2003, 28(4), 313-318